ELSEVIER

Contents lists available at ScienceDirect

Biotribology

journal homepage: www.elsevier.com/locate/biotri





Comparative Tribology: Articulation-induced Rehydration of Cartilage Across Species

Meghan E. Kupratis ^a, Ahmed E. Gure ^c, Kyla F. Ortved ^d, David L. Burris ^{a,b}, Christopher Price ^{a,b,*}

- ^a Biomedical Engineering, University of Delaware, USA
- ^b Mechanical Engineering, University of Delaware, USA
- ^c Bioengineering, University of Texas Arlington, USA
- ^d Clinical Studies, New Bolton Center, University of Pennsylvania, USA

ARTICLE INFO

Keywords:

Articular cartilage tribology Convergent stationary contact area Tribological rehydration Articular cartilage biomechanics Interstitial lubrication Fluid load support

ABSTRACT

Articular cartilage is a robust tissue that facilitates load distribution and wear-free articulation in diarthrodial joints. These biomechanical capabilities are fundamentally tied to tissue hydration, whereby high interstitial fluid pressures and fluid load support facilitate maintenance of low tissue strains and frictions. Our recent ex vivo studies of cartilage sliding biomechanics using the convergent stationary contact area (cSCA) configuration, first introduced by Dowson and colleagues, unexpectedly demonstrated that sliding alone can promote interstitial pressure and lubrication recovery lost to static compression through a mechanism termed 'tribological rehydration.' Although exclusively examined in bovine stifle cartilage to date, we hypothesized that tribological rehydration, i.e., the ability to recover/modulate tissue strains and lubrication through sliding, is a universal articular cartilage behavior. This study aimed to establish if, and to what extent, sliding-induced tribological rehydration is conserved in articular cartilage across a number of preclinical animal species/models and diarthrodial joints. Using a comparative approach, we found that articular cartilage from equine, bovine, ovine, and caprine stifles, and porcine stifle, hip, and tarsal joints all exhibited remarkably consistent sliding speeddependent compression/strain recovery and lubrication behaviors under matched contact stresses (0.25 MPa). All cartilage specimens tested supported robust tribological rehydration during high-speed sliding (>30 mm/s), which as a result of competitive recovery of interstitial lubrication, promoted remarkable decreases in kinetic friction during continuous sliding. The conservation of tribological rehydration across mammalian quadruped articular cartilage suggests that sliding-induced recovery of interstitial hydration represents an important tissue adaptation and largely understudied contributor to the biomechanics of cartilage and joints.

1. Introduction

As the load-bearing biomaterial of diarthroidal joints, articular cartilage supports several key functions, including lubrication, mechanical stiffness, and stress shielding [1–4]. In the absence of injury or disease, cartilage maintains wear-free articulation over decades of repeated loading cycles. These phenomenal biomechanical functions are intimately tied to cartilage hydration. Cartilage is a multiphasic material, comprising ~80% interstitial fluid, a solid extracellular matrix of

anionic glycosaminoglycans and a well-organized collagen scaffold, and a sparsely distributed chondrocyte population [5,6]. Compressive loading pressurizes cartilage's interstitial fluid, shielding the solid matrix from excessive shear and facilitating remarkably low friction during joint motion ($\mu_{eq} \sim 0.005$) through a process known as interstitial lubrication.

Although cartilage's water content is frequently described as a fixed property, it varies with loading state: sustained static compression drives fluid exudation, leading to tissue depressurization and thinning, loss of

Abbreviations: cSCA, convergent stationary contact area; EoS, end-of-sliding; eq, equilibrium state; LME, linear mixed effects model; MCA, migrating contact area; ME, mixed effects model; PBS, phosphate buffered saline; SCA, stationary contact area; SoS, start-of-sliding; δ , compression; ϵ , strain; μ , friction coefficient; τ , characteristic compression/strain/friction recovery time; m, inverse of the characteristic compression/strain/friction recovery time.

^{*} Corresponding author at: 590 Avenue 1743, Newark, DE 19713, USA. *E-mail address:* cprice@udel.edu (C. Price).

interstitial hydration, and the defeat of interstitial lubrication [3,7]. This has been observed ex vivo and in vivo as decreased tissue thickness with compression [3,4,8-10]. Fortunately, clinical imaging studies reveal that joint motion can limit/reverse load-induced cartilage thinning, suggesting an ability of joints to modulate their hydration through activity [10-12]. Through a number of ex vivo studies, we have shown that interstitial fluid exuded from cartilage during static compression, somewhat unexpectedly, can be actively recovered during sliding in the absence of unloading or contact migration [7,8,13-15]. These studies leveraged the convergent stationary contact area (cSCA) cartilage explant testing configuration, which was first used by Dowson and colleagues to study cartilage tribology in a high-speed (up to $\sim \! 100 \ \text{mm}/$ s), hydrodynamic sliding environment [16]. Dowson's initial study concluded that the cSCA response to high-speed sliding was driven by fluid film lubrication, and usage of the configuration largely stalled. Caligaris and Ateshian subsequenty investigated the cSCA configuration in 2008 [2], finding that at slow sliding speeds (1 mm/s), the cSCA behaves no differently from a traditional SCA contact. However, upon revisiting this testing approach under higher sliding speeds in 2017 [7], we found the cSCA to be unique among benchtop testing configurations in its ability to promote the long-term study of cartilage tribomechanics (compressive and sliding biomechanics) across a range of physiologically-informative strain and friction conditions previously inaccessible to 'classical' stationary contact area (SCA) experiments [[7]

As with traditional SCA tests, the cSCA uses osteochondral explants that are compressed and slid against a flat, impermeable glass counterface. However, the cSCA is distinguished from the SCA by its use of convex, large-diameter osteochondral explants, which preserve wedgeshaped convergence zones at the contact periphery [7,13], and we propose that pressurization of bathing solution entrained into these wedges facilitates recovery of interstitial fluid during sliding [4]. This phenomenon, which we have termed tribological rehydration, is characterized by high-speed sliding-driven recovery of tissue volume, and thus, hydration (e.g., interstitial fluid content and pressure) under sustained compressive loading [7,8,17]. Importantly, because of tribological rehydration, the cSCA promotes compression recovery and maintenance of interstitial lubrication, allowing for long-term sustenance, on the benchtop, of physiologically-consistent tissue strains (\sim 5 to 15%) and friction coefficients ($\mu_{eq} < 0.02$) in response to physiologically relevant sliding speeds (~40-100+ mm/s) in the absence of boundary lubricants [8]. Furthermore, the cSCA can achieve low working friction coefficients under constant contact conditions, thereby eliminating contributions from plowing friction that occur in migrating contact area (MCA) configurations[2,18].

Our previous work examined tribological rehydration in bovine (cow) stifle cartilage exclusively, revealing (1) a dependence on contact geometry and sliding speed [4,7], (2) modulation by activity patterning [17], (3) facilitation of solute transport [13,14], and (4) longitudinal reproducibility over several days of repeated testing [8]. However, it is unclear from these findings if sliding-induced tribological rehydration is unique to the bovine model, and if not, whether species-/specimenspecific parameters, such as geometry, scaling, material properties, etc., influence its behavior. For example, Malda et al. found that femoral condyle articular cartilage thickness scales with negative allometry relative to body mass [19]; only deep zone cartilage thickness scales isometrically with body size, the superficial and middle zones scale with negative allometry, suggesting only deep zone adaptation to body size and load bearing [20]. Comparative studies of femoral condyle cartilage biochemical composition [19,20] and aggregate modulus [21] reveal remarkable consistency across mammalian species. Conversely, studies comparing cartilage morphology and mechanical properties among joints report distinct compositional [22–24], mechanical [23,25,26], and transport property differences [22] among articulating surfaces of the knee and ankle.

Despite these findings, comparative approaches have seen limited

use in the exploration of cartilage's lubricating abilities, especially across the large- to moderate-sized model organisms common to articular cartilage biomechanics research. One study reported similar frictional outcomes among cartilage from different bovine stifle compartments [27], and a second, differences among human talar and knee cartilage [26]. In the present study, we aimed to use the cSCA to i) identify if the phenomenon of sliding-induced tribological rehydration is present across articular cartilage from a number of preclinical animal species/models (i.e., equine [species: E.f. caballus; common name: horse], bovine [B. taurus; cow], porcine [S.s. domesticus; domestic pig], ovine [O. aries; sheep], and caprine [C.a. hircus; goat] stifles), and ii) different diarthrodial joints (porcine stifle, hip and tarsal joints), and iii) if there exist global similarities in the sliding-dependent tribomechanical behavior of articular cartilage. We hypothesized that tribological rehydration, and the ability to modulate tissue compression, strains, and lubrication through sliding, is a universal and fundamental behavior of articular cartilage. To test our hypothesis, we used the cSCA configuration to assess cartilage rehydration and lubrication behaviors across different species and joints during sliding under physiologically informative contact stresses and sliding speeds.

2. Methods

2.1. Tissue Specimens

Equine stifles (2 joints from a 4-year-old Thoroughbred mare) were obtained immediately following euthanasia (University of Pennsylvania New Bolton Center, Kennett Square, PA). Bovine and ovine stifles (n = 2& 3, respectively), and a porcine hindlimb were obtained from a local abattoir (Bowman's Butcher Shop, Churchville, MD). A caprine stifle was sourced from a local grocer (Roohani-Lasani Halal Grocery, Newark, DE). Osteochondral explants were extracted with a coring bit from the centerline of each femoral condyle and the articular surface of the porcine femoral head and tibiotalar joint. Explant diameters and locations were chosen to obtain cSCA geometries exhibiting convex curvature (Fig. 1A, Table 1). Explants were rinsed with 1× phosphate buffered saline (PBS), the underlying bone was trimmed to ~15 mm in height using an ISOMET low-speed saw (Buehler, Lake Bluff, IL), and the principal in vivo sliding direction was indicated on each explant. After extraction, explants were stored in a PBS + protease inhibitor solution (5 mM EDTA + 5 mM benzamidine hydrochloride hydrate, Sigma-Aldrich, St. Louis, MO) at 4 °C for no more than 48 h prior to testing.

2.2. Tribological Characterization

A linearly-reciprocating materials testing device (*in situ* tribometer), the operation and capabilities of which have been described previously [7,8], was used in this study. Briefly, cSCA osteochondral explants were compressed and reciprocally slid against a glass microscope slide over a 20-mm track length. In this configuration, a portion of the of the cartilage remains in constant contact with the glass (as in a traditional SCA), while each explant's curvature generates "convergent wedges" at the leading and trailing edges of the contact (Fig. 1A) [28]. During each sliding cycle, cartilage deformation (δ), normal force (F_R), and friction force (F_R), were sampled continuously at 500 Hz. Deformation, normal force, friction force, and kinetic friction coefficient ($\mu_k = F_N/F_F$) were automatically extracted during steady-state sliding over the central 25% of each reciprocation cycle [7]. The data from the positive- and negative-sliding directions were averaged to provide a single data point for each reciprocation cycle.

Within our tribology tests, we aimed to apply consistent pressures to all samples by varying load in response to species-specific differences in sample geometry. A static loading experiment with optical *in situ* contact area measurements was used to determine the loads necessary to obtain target contact pressures of 0.25 \pm 0.05 MPa for each sample group [7]. At the start of tribological testing, a 'run-in' static compression period

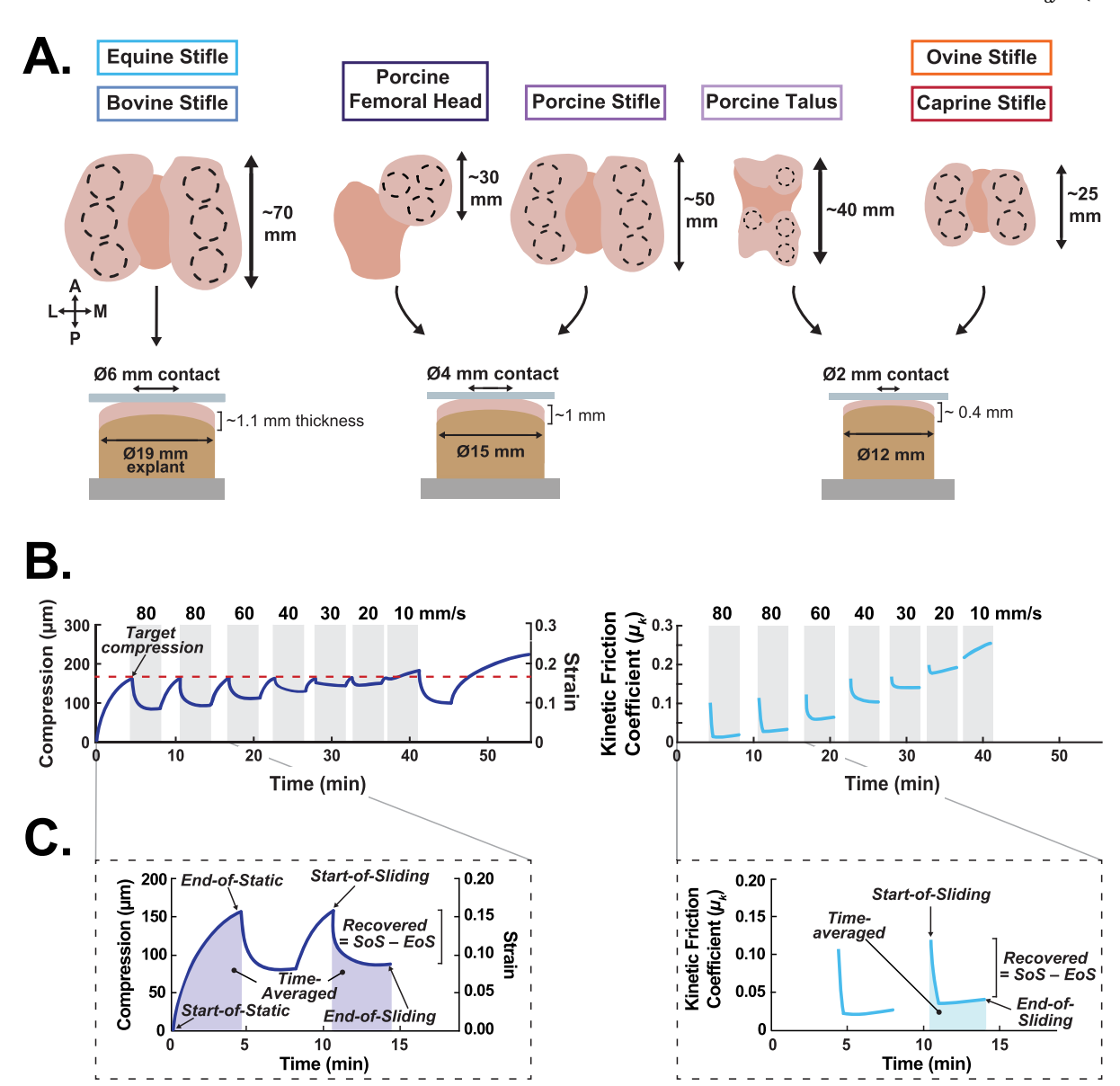


Fig. 1. Experimental design and definition of tribological parameters. A) Schematic illustrating relative sizes of mammalian diarrhrodial joints in the present study and the location and number of cSCA explants extracted from each. Explant diameters were chosen such that macroscopic convex curvature of the cartilage surface was preserved. B) Compression/strain (left) and friction (right) responses of a representative ovine cSCA explant. Tribological testing began with a run-in period of static loading to a target compression value (dotted line) followed by 4 min of sliding at 80 mm/s. Each tribological characterization test comprised a high-to-low speed sweep consisting of repeated 4-min bouts of sliding at 80, 60, 40, 30, 20, and 10 mm/s separated by static compression to the initial target compression value. Each test concluded with a run-out period of sliding at 80 mm/s followed by static loading. White backgrounds correspond to periods of static compression while grey backgrounds correspond to compression plus sliding. C) Tribomechanical parameters extracted from the tests included compression/strain and friction values during the first and last reciprocal sliding cycles (start- and end-of-sliding values, respectively), and time-averaged strain and friction values (area of shaded regions under the curves divided by respective static/sliding duration).

Table 1
Species-dependent cSCA explant geometries, contact areas, and their associated loading conditions.

Species	Common name	Anatomic location	Explant diameter (mm)	Contact area (mm ²)	Applied load (N)	Run-in compression time (min)	Sample size
E.f. caballus (Equine)	Horse	Stifle	19	28 ± 1	7	16	5
B. taurus (Bovine)	Cow	Stifle	19	28 ± 1	7	16	5
S.s. domesticus (Porcine)	Pig	Stifle	15	18 ± 0.5	5	9	5
		Femoral Head	15	7 ± 0.5	2	4	3
		Talus	12	3 ± 0.1	1	2	4
O. aries (Ovine)	Sheep	Stifle	12	7 ± 0.5	2	4	5
C.a. hircus (Caprine)	Goat	Stifle	12	7 ± 0.5	2	4	5

was applied to drive fluid exudation from the cartilage and enable the facile observation of sliding induced tribological rehydration. Because of groupwise differences in explant geometries, the length of these initial static compression periods were scaled (from 2 to 16 min) to allow the application of qualitatively similar tissue strains based upon the classical relationship between the characteristic stress relaxation time for cartilage and the square of the contact radius [5,29]; similar aggregate moduli and permeabilities were assumed among samples. cSCA contact areas, applied loads, and run-in compression times are summarized in Table 1. An exemplar tribology test (ovine stifle sample) consisted of a four-minute 'run-in' (preconditioning) period of static compression (2 N) and 4 min of sliding at 80 mm/s, followed by a high-to-low speed sweep consisting of four-minute sliding bouts at 80, 60, 40, 30, 20, and 10 mm/s. Individual sliding bouts were separated by static compression to the initial deformation of the first static loading period (i.e., the 'runin' static compression; Fig. 1B), and each test concluded with a 4-min sliding 'run-out' at 80 mm/s followed by a static compression period equivalent to the length of the 'run-in' phase. Explants were hydrated with a PBS bath for the duration of testing.

2.3. Data Analysis

All data were processed and analyzed using MATLAB (MathWorks, Natick, MA; 2019a). Following tribomechanical characterization, explants were bisected through the center of the cSCA contact and imaged using a stereomicroscope. Cartilage thickness (h) was measured by tracing the articular cartilage width across each bisected explant and obtaining its average thickness using a Euclidean distance transform. Tribomechanical measurements, including compression (δ) and kinetic friction coefficient (μ_k) were extracted from the raw data (Fig. 1C) as described previously [8]. Tissue strain was defined as $\epsilon = \delta/h$. Compression recovery (and similarly, strain recovery) during each sliding bout was calculated as the difference between the parameter at the start-of-sliding (i.e., the first reciprocal sliding cycle) and the end-ofsliding (i.e., last reciprocal cycle). Kinetic friction coefficients (μ_k) were similarly extracted, and friction recovery during sliding was defined as the difference between μ_k at the start- and end-of-sliding. The sliding speed required to halt net changes in strain recovery and friction coefficient during sliding were defined as the tribological rehydration threshold speed and friction recovery threshold speed, respectively, and were extrapolated from the sliding speed versus strain recovery and friction recovery curves. The tissue's compression/strain and friction response as averaged over each sliding bout (and the initial static loading bout for compression/strain) were calculated as the area under the curve divided by the respective bout duration ('time-averaged' outcomes; Fig. 1C).

We quantified the relative temporal dynamics of sliding-induced tribological rehydration using the curve fitting procedure described by Farnham et al. [8] The sliding-induced compression/strain recovery responses approximate single-phase exponential decay curves, and as such, their kinetics can be described by the generalized exponential expression [$y \approx 1 - e^{-mt}$], where *m* represents the inverse of the characteristic recovery time (τ) , and t is experimental time. The timedependent compression and strain data during each sliding bout were normalized to their respective start-of-sliding values, and the natural log of the resultant exponential decay curves plotted against time. Linear regression fits were performed over the first minute of these compression curves to determine the initial slope (m) of these quasi-linear curves. The constant m reflects the dynamic competition between tribological rehydration and exudation present at the start-of-sliding and can be defined in terms of fluid recovery, where positive m-values (i.e., positive slopes) indicate net tribological rehydration, and negative mvalues indicate net compression induced exudation. Consequently, larger magnitude m-values are indicative of faster exudation or rehydration, while m = 0 indicates no change in compression over time. Similarly, each static compression response took the form of a singlephase exponential association curve [$y \approx e^{mt}$] where exudation due static compression is indicated by negative m values using the convention described above. Using the same approach applied to the sliding curves, start- and end-of-sliding m-values were determined over the first and last minute of the initial static loading period, respectively. Where appropriate, characteristic recovery times (τ) for tribological rehydration and exudation responses are presented as scalar values ($\tau = 1/m$). A similar analysis was performed for friction recovery, except that the linear fits were performed over the first 15 s of sliding to capture the rapid nature of the friction recovery response.

2.4. Statistical Analysis

Statistical analysis was performed with Prism 8 (GraphPad, San Diego, CA) and the R package lme4 (version 1.1.21) [30]. To quantify and compare speed-dependent characteristics of tribological rehydration among samples (i.e., specimens) and groups (i.e., species or joints), mixed effects (ME) models were used to fit tribological outcomes as a function of sliding speed. ME modeling is a statistical approach that systematically accounts for variability explained by an independent variable of interest (fixed effects, e.g., sliding speed) versus random effects (e.g., sample identity) [31]. ME models are particularly useful in 'within-subjects' study designs where repeated measurements are made on the same specimen and then repeated across subsequent specimens and groups. ME model-based analysis is preferred over analysis of variance-based analysis because ME models address data point nonindependence [31,32], thereby accounting for within-subject and within-group variability while establishing population-level relationships between an independent fixed-variable (here, sliding speed) and a dependent outcome (i.e., recovered compression). Compression and strain outcomes were fit using linear mixed effects (LME) models, while friction outcomes were fit using semi-log ME models. The nonparametric Welch's ANOVA with Dunnett's T3 multiple comparisons was used to detect differences in tribological rehydration and friction recovery threshold speeds. The non-parametric Kruskal-Wallis test with Dunn's multiple comparisons was used to detect differences in compression and friction recovery dynamics (m and τ) among groups. In all cases, the threshold for statistical significance was set at multiple comparison adjusted p-value < 0.05.

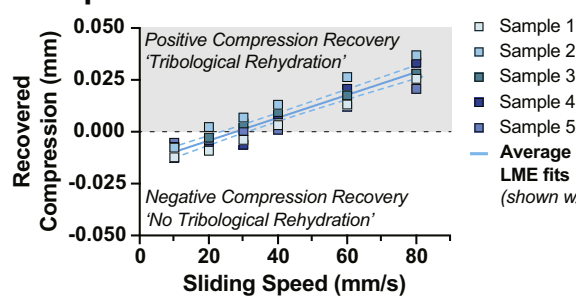
3. Results

3.1. Tribological Rehydration Among Cartilage from Different Mammalian Quadruped Species

We observed tribological rehydration, defined as positive slidingdriven compression and strain recovery with concurrent maintenance of low equilibrium friction coefficients under constant load, across all cSCA cartilage specimens (n = 5 specimens/species for equine, bovine, porcine, ovine, & caprine femoral condyle cartilage). Recovered compression and recovered strain increased linearly as a function of sliding speed in all species (LME *sliding speed*, p < 0.001 for all; Fig. 2–3). Importantly, under similar compressive stresses (~0.25 MPa), changes in compression and strain due to unit increases in sliding speed (i.e., slope of the compression vs. sliding speed curve) were consistent among all specimens within a group (LME slopes were statistically indistinguishable among specimens for a given species, p > 0.05; Fig. 2A–E & Fig. 3A-E, respectively). Minor differences in recovery magnitudes were attributable to the superposition of these shared compression/strain versus sliding speed relationships upon meaningful initial interspecimen variability (LME intercepts differed among specimens; sample identity effect, p < 0.001). Similar assessments of end-of-sliding and time-averaged compressions and strains can be found in Supplemental Fig. 1 and 2, respectively.

Given the overall consistency of compression and strain responses within each species, group datasets could be collapsed to their shared

A. Equine

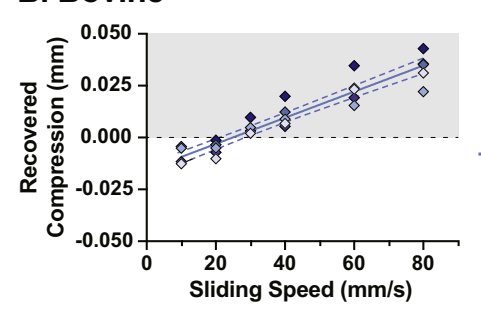


LME Model

Sliding speed effect: p < 0.001

- · No diff. in slopes among specimens (p = 0.11)
- Ava. slope = 5.50E-4 mm/[mm/s] Sample identity effect: p < 0.001

B. Bovine



Sample 1 LME Model Sample 2 Sliding speed effect: p < 0.001Sample 3

Sample 2

Sample 3

Sample 4

Sample 5

I MF fits

Sample 4

Sample 5

LME fits

Average of

(shown w/ 95% CI)

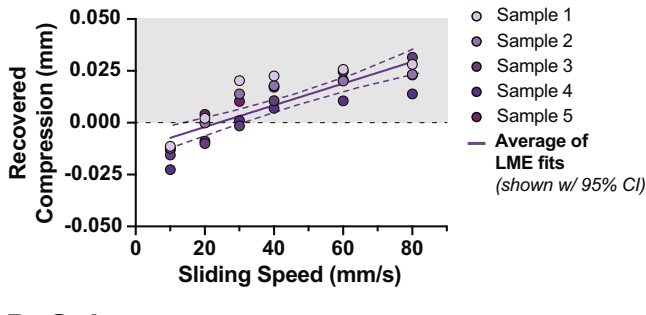
Average of

(shown w/ 95% CI)

- No diff. in slopes among specimens (p = 0.06)
- Avg. slope = 6.29E-4 mm/[mm/s] Sample identity effect: p < 0.001

Fig. 2. Overall consistency in slidinginduced compression recovery responses were observed for femoral condyle articular cartilage of each species tested. Recovered compression increased linearly with sliding speed for all specimens and species (i.e., sliding speed effect). Positive compression recovery (grey shaded regions) indicates tribological rehydration, while negative recovery (white) indicates net load-induced compression. LME model analysis indicated that within each species, specimens shared similar recovered compression versus sliding-speed relationships (i.e., LME slopes were statistically indistinguishable among specimens) despite being superimposed upon meaningful inter-specimen variability (LME intercepts statistically differed among specimens, sample identity effect). The slope of the shared LME model for each species (solid lines) and the 95% confidence intervals for each slope (dotted lines) are shown, and the parameters describing each model are provided to the right of each panel.

C. Porcine

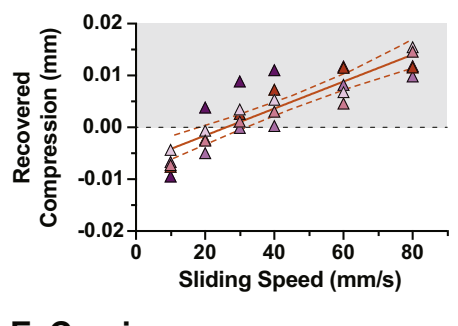


LME Model

Sliding speed effect: p < 0.001

- · No diff. in slopes among specimens (p = 0.53)
- Avg. slope = 5.24E-4 mm/[mm/s] Sample identity effect: p < 0.001

D. Ovine



Sample 1 Sample 2

Sample 3 Sample 4

Sample 5 Average of I MF fits

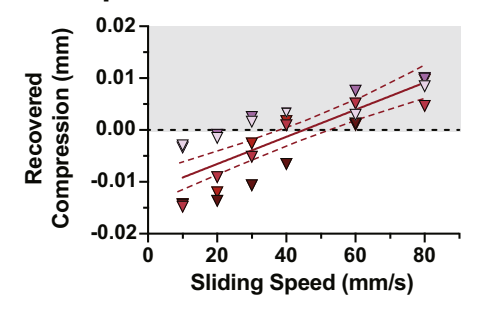
(shown w/ 95% CI)

LME Model

Sliding speed effect: p < 0.001

- · No diff. in slopes among specimens (p = 0.99)
- Ava. slope = 6.77E-3 mm/lmm/sl Sample identity effect: p < 0.001

E. Caprine



Sample 1 Sample 2 Sample 3 Sample 4

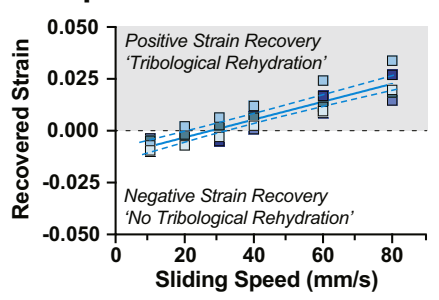
Sample 5 Average of LME fits (shown w/ 95% CI)

LME Model

Sliding speed effect: p < 0.001

- · No diff. in slopes among specimens (p = 0.07)
- Avg. slope = 2.62E-4 mm/[mm/s] Sample identity effect: p < 0.001

A. Equine



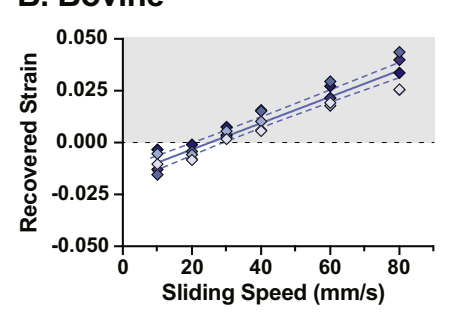
Sample 1 LME Model Sample 2

Sliding speed effect: p < 0.001

- No diff. in slopes among specimens (p = 0.31)
- Ava. slope = 4.31E-4 1/Imm/sl Sample identity effect: p < 0.001

(shown w/ 95% CI)

B. Bovine



Sample 1 Sample 2 Sample 3

Sample 3

Sample 4

Sample 5

LME fits

Average of

Sample 4 Sample 5

Average of LME fits (shown w/ 95% CI)

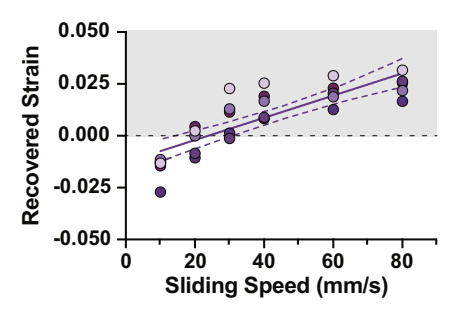
LME Model

Sliding speed effect: p < 0.001

- · No diff. in slopes among specimens (p = 0.25)
- Avg. slope = 6.35E-4 1/[mm/s] Sample identity effect: p < 0.001

Fig. 3. Similarly, consistency in femoral condyle articular cartilage strain recovery responses during sliding were observed for each species tested. Recovered strain increased linearly with sliding speed for all specimens across all species. Positive strain recovery (grey shaded regions) indicates tribological rehydration, while negative recovery (white) indicates net load-induced compression. LME model analysis indicated that within each species, specimens shared similar recovered strain versus sliding-speed relationships despite meaningful underlying inter-specimen variability. The slope of the shared LME model for each species (solid lines) and the 95% confidence intervals for each slope (dotted lines) are shown, and the parameters describing each model are provided to the right of each panel.

C. Porcine



Sample 1 Sample 2

Sample 3 Sample 4

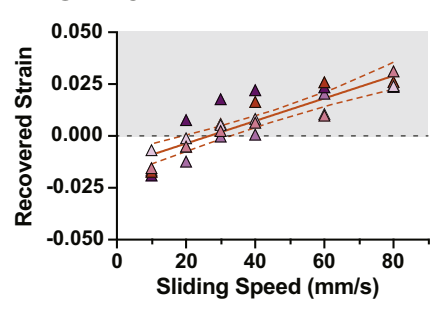
Sample 5 Average of LME fits (shown w/ 95% CI)

LME Model

Sliding speed effect: p < 0.001

- · No diff. in slopes among specimens (p = 0.95)
- Avg. slope = 5.36E-4 mm/[mm/s] Sample identity effect: p < 0.001

D. Ovine



Sample 1 Sample 2

Sample 3

Sample 4

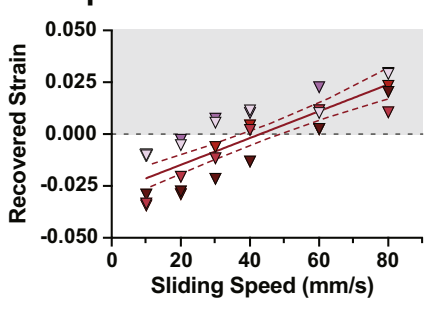
Sample 5 Average of LME fits (shown w/ 95% CI)

LME Model

Sliding speed effect: p < 0.001

- · No diff. in slopes among specimens (p = 0.65)
- Avg. slope = 5.44E-4 mm/[mm/s] Sample identity effect: p < 0.001

E. Caprine



Sample 1

Sample 2 Sample 3

Sample 4 Sample 5

Average of LME fits (shown w/ 95% CI)

LME Model

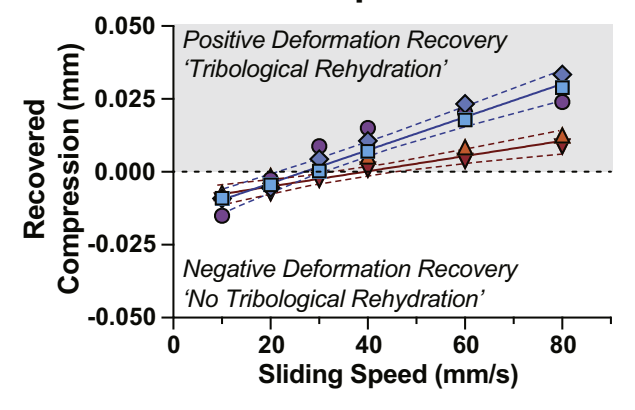
Sliding speed effect: p < 0.001

- · No diff. in slopes among specimens (p = 0.36)
- Avg. slope = 6.46E-4 mm/[mm/s] Sample identity effect: p < 0.001

species-specific LME models to facilitate and visualize a comparative analysis among species (see Fig. 4). This treatment highlighted several interesting behaviors in response to cSCA sliding speed. Comparison of the mean compression and strain recovery responses (Fig. 4A-B) demonstrated that their recovery increased linearly with sliding-speed

across all species (p < 0.001). Equine, bovine, and porcine stifle cartilage samples, overall, exhibited significantly greater compression recovery per unit change in sliding speed (pooled slope = 4.09E-5 mm• (mm/s) $^{-1}$ [LME Model 1] vs. 2.78E-5 mm• (mm/s) $^{-1}$ [LME Model 2, ovine and caprine stifle cartilage]; Fig. 4A). However, when recovered

A. Recovered Compression



LME slopes differ among species:

p < 0.001

— LME Model 1

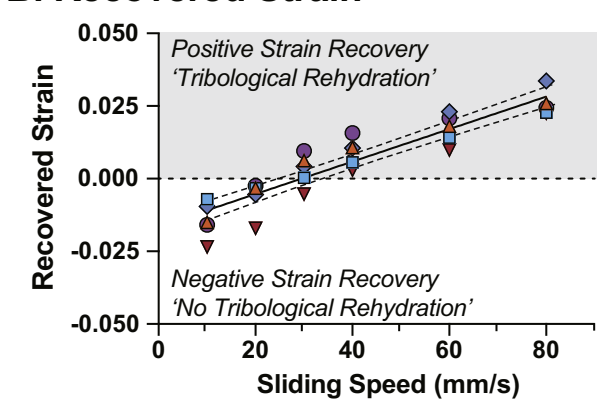
(Equine, Bovine, Porcine) **Sliding speed effect:** p < 0.001• Avg. slope = 5.68E-4 mm/[mm/s] **No species effect:** p = 0.47

— LME Model 2

(Ovine, Caprine)

Sliding speed effect: p < 0.001 • Avg. slope = 2.61E-4 mm/[mm/s] Species effect: p < 0.001

B. Recovered Strain



No diff. in LME slopes among species:

p = 0.32

— LME Model

Sliding speed effect: p < 0.001 • Avg. slope = 5.58E-4 mm/[mm/s] **Species effect:** p < 0.001



C. Tribological Rehydration Threshold Speed

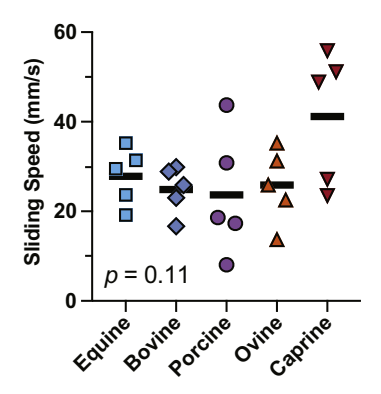


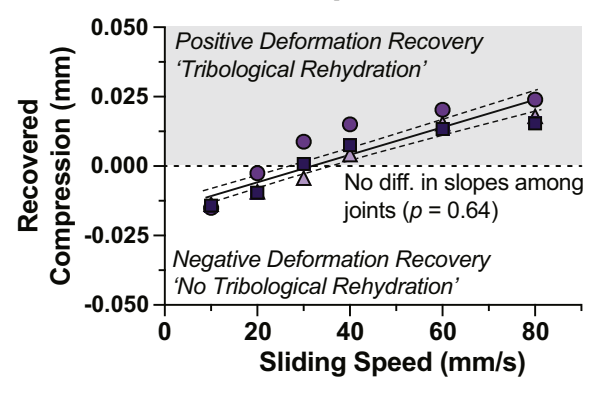
Fig. 4. Speed-dependent femoral condyle articular cartilage compression and strain recovery behaviors across species. A) Compression recovery responses from Fig. 2 were collapsed to their respective species means to facilitate comparative analyses of tribological rehydration behaviors among species, revealing two different compression recovery behavior trajectories (different LME slopes, p < 0.001; LME1 – equine, bovine, & porcine, and LME2 – ovine and caprine). The slope of each shared LME model (solid lines) and the 95% confidence intervals for each slope (dotted lines) are shown, and the parameters describing each model are provided to the right of each panel. B) Similarly, strain recovery responses from Fig. 3 were collapsed to the respective species means to facilitate comparative analyses of tribological rehydration behaviors among species, revealing a single globally-consistent, or species-independent strain recovery behavior under sliding. C) The predicted speed at which sliding-induced rehydration balanced load-induced exudation were extrapolated from LME models; these tribological rehydration threshold speeds were statistically indistinguishable among species (p = 0.11).

compression was normalized to tissue thickness (i.e., analyzed in terms of recovered strain, Fig. 4B) species-dependent variability in this relationship disappeared (p=0.32; pooled slope = 5.58E-4 (mm/s) $^{-1}$). Accordingly, both end-of-sliding and time-averaged compression and strain decreased linearly as sliding-speed increased—a clear indication of increasing tribological rehydration with higher sliding speeds.

Cartilage from larger species generally exhibited greater end-of-sliding compression and smaller end-of-sliding strain magnitudes at all sliding speeds under 0.25 MPa compressive stress. The LME model fits for end-of-sliding and time-averaged compression/strain behavior can be found in Supplemental Fig. 3.

Compression and strain recovery temporal dynamics were described

A. Recovered Compression



No diff. in LME slopes among joints: p = 0.64

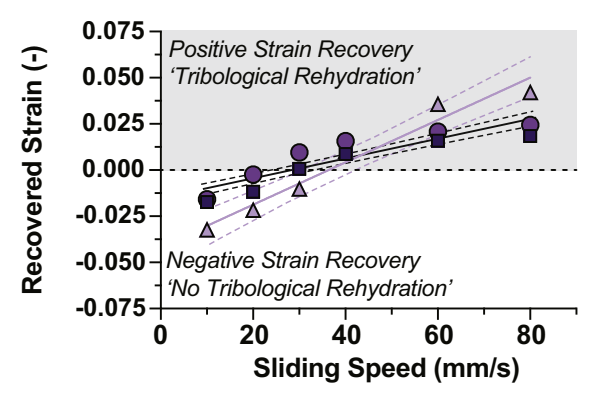
— LME Model

Sliding speed effect: p < 0.001

• Avg. slope = 4.91E-4 mm/[mm/s]

Joint effect: p = 0.002

B. Recovered Strain



LME slopes differ among joints:

p < 0.001— LME Model 1(Talus)

Sliding speed effect: p < 0.001

Avg. slope = 1.15E-3 1/[mm/s]

— LME Model 2 (Femoral Head, Stifle)
Sliding speed effect: p < 0.001</p>

• Avg. slope = 5.33E-4 1/[mm/s] **Joint effect:** p = 0.01

■ Femoral Head ● Stifle ▲ Talus

C. Tribological Rehydration Threshold Speed

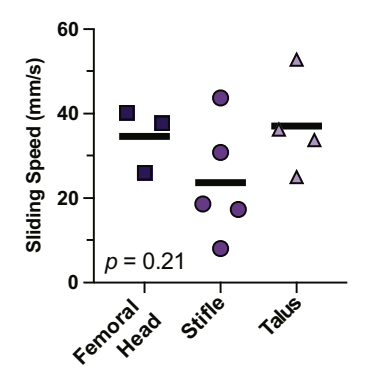


Fig. 5. Speed-dependent compression and strain recovery behavior across articular cartilage explants from hindlimb joints of a single porcine subject. A) Compression recovery outcomes from Supp. Fig. 5 were collapsed to their respective joint-specific shared responses to facilitate comparative analyses of tribological rehydration behaviors among different porcine hindlimb joints (femoral head, stifle, and talus). A consistent, or joint identity-independent, compression recovery vs. sliding speed relationship was observed across all three joints. The slope of each shared LME model (solid line) and the 95% confidence intervals for each slope (dotted lines) are shown, and the parameters describing each model are provided to the right of each panel. B) Average strain recovery responses of porcine femoral head, stifle, and talus cSCA explants. Speed-dependent compression recovery increased linearly and consistently among the three joints; however, talus explants underwent greater strain recovery per unit increase in sliding speed than femoral head and stifle explants. C) Tribological rehydration threshold speeds, or the sliding speeds at which sliding-induced recovery and load-induced exudation are equivalent, were statistically indistinguishable among porcine hindlimb joints (p = 0.21).

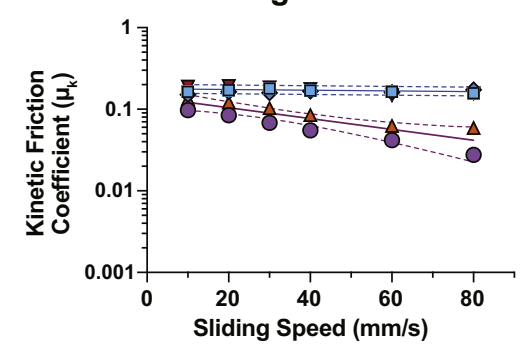
by the inverse characteristic recovery time m. By convention, negative m-values indicate net compression during sliding (and static loading), while positive m-values indicate sliding-driven recovery of load-induced compression. In all samples and species, m increased linearly with sliding speed (p < 0.001), transitioning from negative to positive values at intermediate speeds (20–40 mm/s). Overall, the influence of unit changes in sliding speed on changes in compression recovery dynamics were quite consistent among equine, bovine, and ovine explants, while porcine and caprine samples tended to have $\sim 50\%$ higher and lower slopes, respectively (p < 0.001, Supplemental Fig. 4). Interestingly, among all species, tribological rehydration threshold speeds—the predicted speeds at which sliding-induced rehydration precisely balanced compression-induced exudation in the cSCA; i.e., recovered compression and strain, and $m \approx 0$ — were consistent among species (x-intercepts = 24–41 mm/s, p = 0.11; Fig. 4C).

3.2. Tribological Rehydration Among Hindlimb Diarthrodial Joints

We also examined the tribomechanical behavior of cSCA explants

from three joints (femoral head, stifle, and talar articular cartilage) of a single porcine hindlimb. These tests revealed a consistent, linear relationship between sliding speed and compression recovery (i.e., tribological rehydration; sliding speed effect, p < 0.001; no difference in slopes, p = 0.64), despite a dependence of compression recovery magnitudes upon anatomic site (sample identity effect, p < 0.002; Fig. 5A). Additionally, sliding speed-dependent changes in end-of-sliding compression (and strain) were indistinguishable among different hindlimb joint (p = 0.19 & 0.49, respectively; Supplemental Fig. 5), despite end-of-sliding magnitudes varying among joints (p < 0.001). Interestingly, relative strain recovery (per unit change in sliding speed) was marginally greater in porcine talar cartilage (Fig. 5B). The timeaveraged compression and strain behaviors mirrored those of the stifle cartilage specimens, decreasing linearly with sliding speed in all samples (Supplemental Fig. 6). When collapsed to their respective group means, speed-dependent time-average compression outcomes were indistinguishable among joints, while talar explants exhibited greater relative changes in time-averaged strain (Supplemental Fig. 7). Finally, the initial compression and strain recovery kinetics increased with sliding

A. Start-of-Sliding Friction

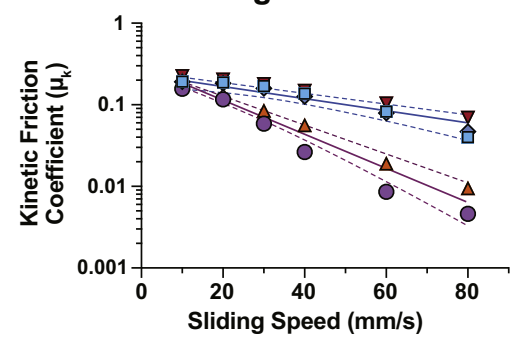


ME slopes differ among species: p = 0.001

— ME Model 1
(Equine, Bovine, Caprine)
No sliding speed effect: p = 0.13
Species effect: p < 0.001

ME Model 2 (Porcine, Ovine)
Sliding speed effect: p < 0.001
Avg. slope = -6.64E-3 1/[mm/s]
Species effect: p < 0.001

B. End-of-Sliding Friction



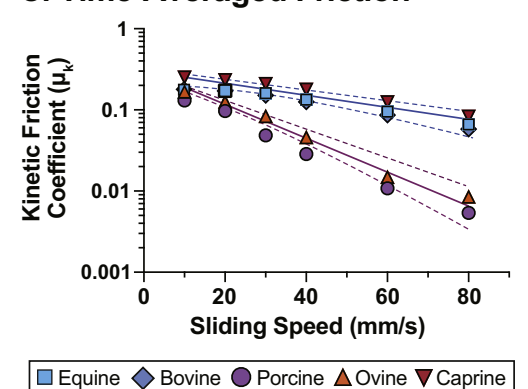
ME slopes differ among species: p < 0.001

ME Model 1
(Equine, Bovine, Caprine)
Sliding speed effect: p < 0.001
Avg. slope = -7.36E-3 1/[mm/s]
Species effect: p = 0.006

ME Model 2 (Porcine, Ovine)
Sliding speed effect: p < 0.001
Avg. slope = -2.01E-2 1/[mm/s]
No species effect: p = 0.13

Fig. 6. Sliding-speed dependent femoral condyle cartilage friction outcomes among species. Kinetic friction outcomes from Supp. Fig. 9 were collapsed to their respective mean species-specific responses to permit comparative analyses of speed-dependent frictional behaviors. A) High start-of-sliding friction coefficients were observed at all sliding speeds across all species. Sliding speed had no significant effect on start-of-sliding friction coefficients in equine, bovine, or caprine stifle cSCA explants (ME Model 1); however, start-of-sliding friction did decrease with increasing sliding speeds for porcine and ovine cSCA explants (ME Model 2). B&C) End-of-sliding and time-average friction coefficients decreased dramatically with increasing sliding speed for all species. Similar to the start-of-sliding response, greater proportional suppression of end-of-sliding and timeaverage friction occurred for porcine and ovine cSCA explants (ME Model 2) relative to bovine, equine, and caprine explants (ME Model 1). The slopes of the shared ME models (solid lines) and the 95% confidence intervals for each shared slope (dotted lines) are shown, and the parameters describing each model are provided to the right of each panel.

C. Time-Averaged Friction



ME slopes differ among species: p < 0.001

— ME Model 1
(Equine, Bovine, Caprine)

Sliding speed effect: p < 0.00

Sliding speed effect: p < 0.001
• Avg. slope = -6.18E-3 1/[mm/s]
Species effect: p < 0.001

ME Model 2 (Porcine, Ovine)
Sliding speed effect: p < 0.001
Avg. slope = -1.84E-2 1/[mm/s]
No species effect: p = 0.12

speed (Supplemental Fig. 8), albeit with more inter-joint variability. Nonetheless, predicted tribological rehydration threshold speeds were quite consistent among specimens from the different hindlimb joints (x-intercepts = 24–37 mm/s, p = 0.21; Fig. 5C).

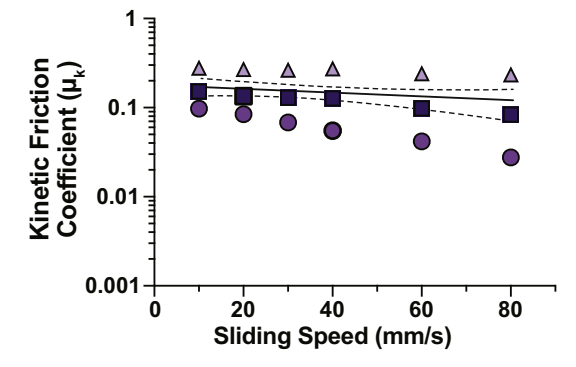
3.3. Sliding Speed-Dependent cSCA Frictional Behaviors Across Species and Joints

Figs. 6 and 7 show the mean start-of-sliding, end-of-sliding, and time-averaged kinetic friction coefficients as a function of sliding speed for femoral condyle cartilage from the different species and porcine hindlimb joints, respectively. After each bout of static compression, moderate to very high start-of-sliding kinetic friction coefficient values were always observed during the first sliding cycle at all speeds and in all specimens ($\mu_{SoS} = 0.04-0.31$; Figs. 6A & 7A). With continued sliding,

kinetic friction values decreased significantly at sliding speeds ≥ 40 mm/s (p<0.001, Wilcoxon matched pairs sign rank test between start- and end-of-sliding friction coefficients), achieving markedly low values by the end-of-sliding at the fastest speeds tested: $\mu_{EoS}=0.008-0.13$ at 60 mm/s and $\mu_{EoS}=0.004-0.09$ at 80 mm/s (Figs. 6B & 7B). Notably, such low friction values were achieved in the presence of PBS only, which is consistent with all prior cSCA-based studies [4,7,8,13,14,16,17]. Of equal importance, time-averaged friction coefficients were maintained at low magnitudes ($\mu_{TA}<0.1$) for sliding speeds ≥ 30 mm/s across all specimens (Figs. 6C & 7C), indicating that exposure to high initial friction is a transient phenomenon when cSCA explants are slid at moderate to high sliding speeds. Raw friction data for all specimens from each species/joint can be found in Supplemental Figs. 9 & 10.

Sliding speed had no significant effect on start-of-sliding friction coefficients in equine, bovine, and caprine stifle explants, (semi-log ME

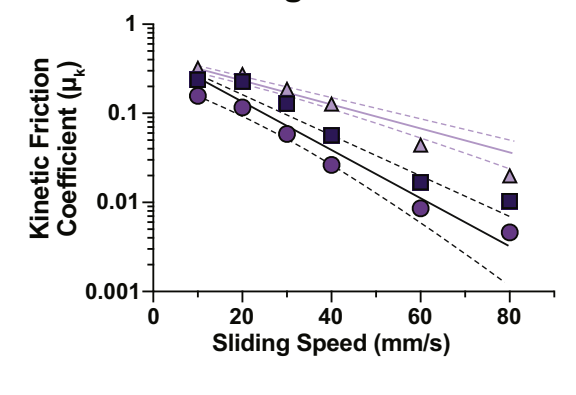
A. Start-of-Sliding Friction



No diff. in ME slopes among joints: p = 0.09

ME Model
Sliding speed effect: p = 0.01
Avg. slope = -5.93E-3 1/[mm/s]
Joint effect: p < 0.001

B. End-of-Sliding Friction



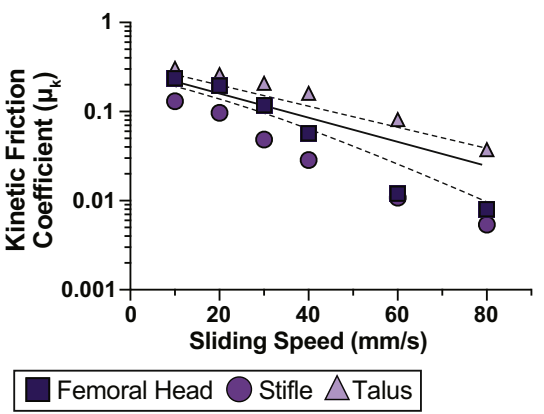
ME slopes differ among joints: p < 0.001

ME Model 1 (Talus)
Sliding speed effect: p < 0.001
Avg. slope = -9.35E-3 1/[mm/s]

ME Model 2 (Porcine, Ovine)
Sliding speed effect: p < 0.001
Avg. slope = -1.80E-2 1/[mm/s]
No joint effect: p = 0.21

Fig. 7. Speed-dependent friction behavior across articular cartilage explants from hindlimb joints of a single porcine subject. Kinetic friction outcomes from Supp. Fig. 10 were collapsed to their respective jointspecific mean responses to facilitate comparative analyses among different porcine hindlimb joints (femoral head, stifle, and talus). A&C) Sliding speeddependent start-of-sliding and timeaveraged friction responses were consistent among porcine hindlimb joints (no diff. in slopes); B) however, speed-dependent decreases in end-of-sliding friction coefficients were greater in femoral head and stifle explants (ME Model 2) relative to talus explants (ME Model 1). The slopes of the shared ME models (solid lines) and the 95% confidence intervals for each shared slope (dotted lines) are shown, and the parameters describing each model are provided to the right of each panel.

C. Time-Averaged Friction



No diff. in ME slopes among joints: p = 0.05

ME Model
Sliding speed effect: p < 0.001
Avg. slope = -1.39E-2 1/[mm/s]
Joint effect: p = 0.03

modeling; sliding speed effect, p=0.13; Fig. 6A); however, decreases in start-of-sliding friction with sliding speed were observed for porcine and ovine specimens (p<0.001). While end-of-sliding friction coefficients decreased in a sliding speed-dependent manner across all species (p<0.001), greater reductions in end-of-sliding (and time-average) friction coefficients per unit increase in sliding speed were observed for porcine and ovine specimens (p<0.001; Fig. 6B).

Among different porcine hindlimb joints, increases in sliding speed resulted in modest reductions in start-of-sliding friction coefficients (p=0.01; Fig. 7A), and far more robust reductions in end-of-sliding and time-averaged friction coefficients (p<0.001; Fig. 7B). Joint identity had a significant effect on speed-dependent start-of-sliding and time-average friction magnitudes (p<0.001 & p=0.027, respectively; Fig. 7A&C), but not the slopes of these relationships (p=0.091 & 0.052, respectively). In contrast, changes in end-of-sliding friction coefficients per unit increase in sliding speed were greater in femoral head and stifle cartilage than talus cartilage (p<0.001; Fig. 7B). Overall, talar cartilage cSCA explants generally exhibited elevated frictional behaviors in response to sliding.

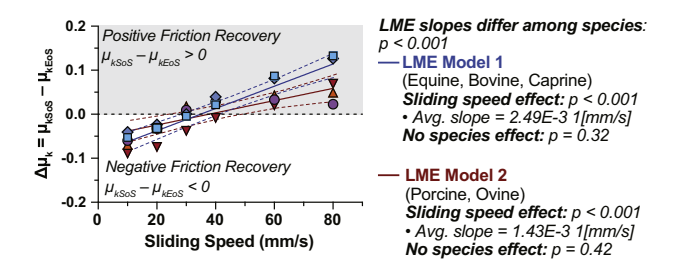
Changes in friction magnitude between the start- and end-of-sliding for a given sliding speed, referred to as the friction recovery response, mirrored the species-dependent end-of-sliding and time-average frictional outcomes. At slow sliding speeds (≤ 20 mm/s), negative friction recoveries were universally seen, indicating unmitigated increases in friction coefficients with sliding across all specimens (Fig. 8A). Friction recovery increased linearly with sliding speed (p < 0.001), and positive friction recoveries accompanied sliding at ≥ 50 mm/s. Interestingly, proportionally greater friction recovery occurred among equine, bovine,

and caprine specimens (LME Model 1) for unit changes in sliding speed than porcine and ovine specimens (LME Model 2, different slopes, p < 0.001; Fig. 8A). Minor, but statistically significant, differences in friction recovery threshold speeds-defined as the predicted speed at which kinetic friction values remain unchanged after initiating sliding (i.e., $\mu_{SoS} - \mu_{EoS} = 0$)—were observed between species, with caprine specimens requiring faster sliding speeds to suppress kinetic friction during sliding than equine and bovine specimens (p = 0.02 and 0.006, respectively; Fig. 8B). Assessment of the temporal dynamics of frictional recovery demonstrated the rapidity with which high-speed sliding suppresses interfacial frictions (Fig. 8C). At 80 mm/s, characteristic friction recovery times (7) ranged from 0.11 to 0.78 min, with frictional suppression being faster in porcine and ovine stifle explants (p < 0.02, Kruskal-Wallis test). Speed-dependent friction recovery behaviors, friction recovery threshold speeds, and characteristic friction recovery times were indistinguishable among the specimens from the different porcine hindlimb joints (Fig. 8D-F).

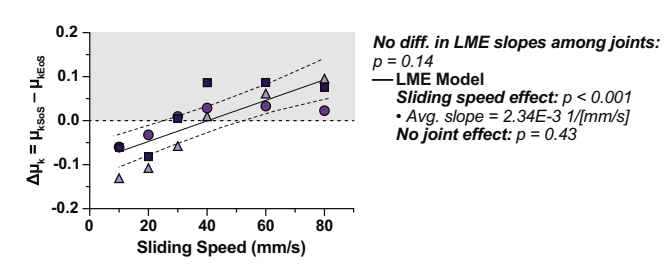
4. Discussion

In the present study, we sought to confirm if, and to what extent, articular cartilage from different mammalian species and joints supports tribological rehydration [7], a sliding-dependent biomechanical phenomenon suspected to contribute to the recovery and sustenance of cartilage hydration and tribomechanical function by joint activity [13,15]. The discovery of tribological rehydration was an unanticipated consequence of revisiting the *in situ* convergent stationary contact area (cSCA) cartilage testing configuration that Dowson and colleagues first

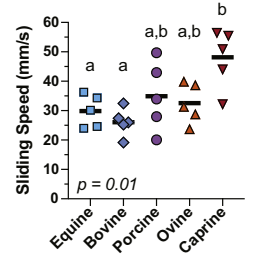
A. Friction Recovery

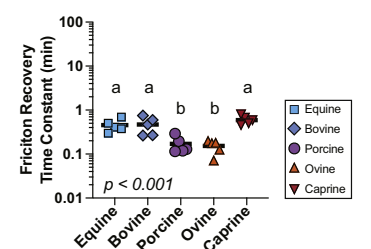


D. Friction Recovery



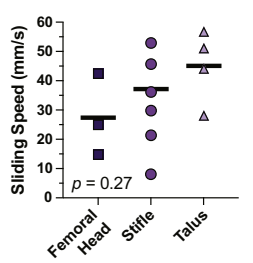
B. Friction Recovery C. High-Speed Friction Threshold Speed Recovery Time Constant





E. Friction Recovery Threshold Speed

F. High-Speed Friction Recovery Time Constant



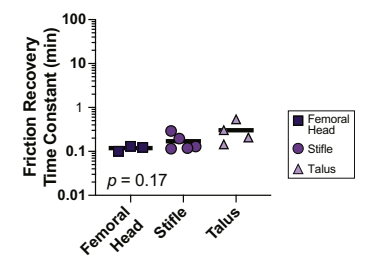


Fig. 8. Speed-dependent friction behaviors of articular cartilage explants across species and joints. A) The friction recovery response of cSCA articular cartilage, defined as the change in friction magnitude from start- to end-of-sliding, increased with sliding speeds across all species. Positive friction recovery (i.e., net decrease in friction during sliding) is indicated by the grey background. For stifle cartilage, proportionally greater friction recovery was observed for equine, bovine, and caprine cSCA explants (LME Model 1) relative to porcine and ovine explants (LME Model 2). The slopes of the shared LME models (solid lines) and the 95% confidence intervals for each shared slope (dotted lines) are shown, and the parameters describing each model are provided to the right of each panel. B) Extrapolated friction recovery threshold speeds, defined as the predicted sliding speed at which the no net change in friction would occur, were slowest for equine and bovine specimens and fastest for caprine specimens (p = 0.02, equine vs. caprine and p = 0.005, bovine vs. caprine, Welch's ANOVA with Dunnett's multiple comparisons test; groups having dissimilar letters represent pairs that are statistically different from one another). C) Temporal dynamics of friction recovery at 80 mm/s. Friction suppression occurred very rapidly upon the initiation of 80 mm/s sliding; somewhat faster friction suppression was observed in porcine and ovine stifle explants than equine, bovine, or caprine explants (p < 0.02, Kruskal-Wallis test with Dunn's multiple comparisons). D—F) Speed-dependent friction recovery behaviors, friction recovery threshold speeds, and high-speed friction recovery time constants were indistinguishable among porcine hindlimb joints.

introduced decades ago to study the hydrodynamic environment of the joint [16]. Because the authors of that study defeated interstitial pressure prior to sliding, they concluded that the drastic friction reductions observed during high-speed sliding of the cSCA were due to hydrodynamic fluid film-based lubrication effects. Contrary to the assumption that pore pressure remains insignificant during cSCA sliding following static equilibration, we have shown recently that the cSCA's hydrodynamic environment induces tribological rehydration [4,7], which restores interstitial hydration, pore pressure, and interstitial lubrication during sliding [4,7,8,15]. Furthermore, we have demonstrated conclusively that tribological rehydration is a speed-dependent phenomenon that sustains interstitial lubrication without introducing unpredictable/ unquantifiable contribution from bath exposure, contact migration, or plowing friction. However, all of our cSCA-based tribological rehydration studies to date had been restricted to bovine stifle (i.e., femoral condyle) cartilage. While there was no reason to suspect, a priori, that tribological rehydration should be restricted solely to bovine femoral condyle cartilage tissues, it had yet to be tested in cartilage explants from other species and joints. This comparative tribology study represents the first of its kind to demonstrate the universality and qualitative consistency of sliding-induced tribological rehydration across a range of model organisms (including: equine [species: E.f. caballus; common name: horse], bovine [B. taurus; cow], porcine [S.s. domesticus; domestic pig], ovine [O. aries; sheep], and caprine [C.a. hircus; goat] stifle, and joints (porcine femoral head, stifle, and tarsal).

All specimens tested in this study exhibited robust articulationinduced tribological rehydration at higher sliding speeds (40-80 mm/ s) and under similar constant compressive stresses (~0.25 MPa). It should be noted that while articular cartilage in the knee can be subject to peak compressive stresses on the order of 10–20 MPa during activities like walking [10,17,33-35], such high contact pressures occur transiently, with contact pressures varying constantly in magnitude and location over the gait cycle [36,37]. Furthermore, since cartilage is composed predominately of incompressible water, subjecting the tissue to rapid cyclic loading generates high levels of interstitial fluid pressurization and fluid load support (>95%) [38], which in accordance with interstitial lubrication theory, affords cartilage remarkable lubricity when loads/stresses are applied (and then removed) faster than the tissue can depressurize [3,5,39]. Thus, in well-hydrated cartilage, rapidly and transiently applied peak loads have little bearing on overall cartilage lubricity. In fact, cartilage appears to be supremely resistant (and insensitive) to rapidly cycled loading. Instead, it is the average contact stress experienced by articular cartilage that dictates the tissue's tribomechanical response [33]. Importantly, spatially- and temporallyaveraged contact stresses within mammalian joints are highly consistent, ranging from ~0.1–2.0 MPa [10,40]. Accordingly, the choice of an experimental compressive stress of ~ 0.25 MPa is fully consistent with average articular cartilage contact stresses registered in vivo and subsequently determinative of overall tribomechanical behaviors. Extensive studies of articular cartilage tribology have been performed under slowspeed sliding conditions (typically ≤ 10 mm/s) [2,41–47]. Based on this precedence, some might consider the sliding speeds utilized herein (10-80 mm/s) to be 'high' for benchtop studies. However, these speeds are quite consistent with tangential articulation (sliding/gliding) speeds during gait (mean speeds in the range of 50 mm/s and maximum speeds of 150 mm/s) [17,48], and are highly conserved among large mammalian species [49–51]. Thus, the compressive pressure and range of sliding speeds utilized in the present study can be considered physiologically relevant and informative with regards to both the our chosen model species and human locomotion.

Sliding speed-dependent characteristics of: i) compression/strain recovery (i.e., tribological rehydration), and ii) cartilage lubrication modulation were remarkably consistent among species (and among porcine hindlimb joints), demonstrating the *robust* and *immutable* nature of sliding-induced tribological rehydration and recovery of tribomechanical behavior across mammalian quadruped articular cartilage.

Nonetheless, we did identify species-dependent and -independent behaviors across our cSCA sliding tests. Although species identity dictated end-of-sliding and recovered compression magnitudes throughout our tests, noteworthy consistency in sliding-dependent compression and strain recovery behavior was observed. Importantly, the speeddependent strain recovery outcomes were statisticallyindistinguishable among all the stifle cartilage samples. Across species, the predicted sliding speeds at which compression-induced exudation and sliding-induced rehydration were in perfect balance, termed tribological rehydration threshold speed, were incredibly consistent (~30 mm/ s). Thus, under an average compressive stress of 0.25 MPa, sliding at >30 mm/s favors rehydration over exudation, and, as indicated below, net decreases in friction. Again, it must be noted that this threshold speed falls below the average articulation speed of human (~50 mm/s) [17,52] and various quadruped (~45 mm/s) [36,49,50,53,54] joints during walking gaits. This suggests that in the face of physiologically consistent temporally-averaged contact stresses (0.1–2 MPa) [40,55], typical joint motions should be adequate for supporting articulationmediated recovery of cartilage thickness through tribological rehydration [10,11].

Although all cSCA stifle explants exhibited qualitatively similar strain behaviors during the static and sliding phases of our tests, differences in the temporal dynamics of both load-induced fluid exudation during the static phases and sliding-induced fluid recovery were observed. Fig. 9 highlights difference in the temporal dynamics (i.e., kinetics) of strain responses across species at the start- and end-of-static loading, and during the start-of-sliding at 10 and 80 mm/s. While m values (or equivalently, rates of static compression-induced strain accumulation) at the end of static compression were consistent among species (p = 0.24, Welch's ANOVA), tissues that strained more quickly over the first minute of static loading appeared to recover strain faster upon the initiation of high-speed sliding (p < 0.001, Welch's ANOVA). Additionally, from this visualization, it is easily appreciated that measurable fluid recovery actually occurs at slow sliding speeds: when

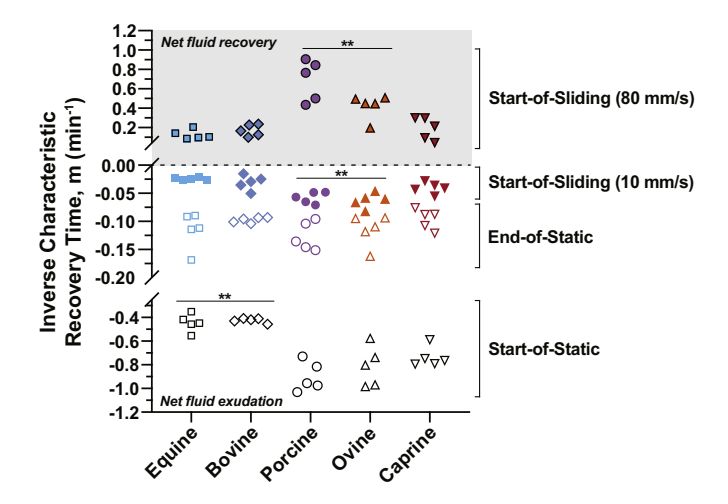


Fig. 9. Comparison of species-dependent strain recovery dynamics across selected compression and sliding conditions. Comparative analysis of the temporal dynamics of load-induced exudation and sliding-induced rehydration revealed both species-dependent and species-independent responses. Equine and bovine cSCA explants strained faster than porcine, ovine, and caprine stifle specimens over the first minute of static compression at 0.25 MPa (m-values were more negative); however, exudation rates as the tissue neared equilibrium (calculated over the last minute of static loading) were indistinguishable among species. Porcine and ovine explants exhibited significantly faster exudation (greater negative strain recovery rates) at slow speeds and faster rehydration (greater positive strain recovery rates) at high speeds. Groups whose m values are significantly different from the other groups under the same sliding conditions are denoted with asterisks (**p< 0.001).

slid at 10 mm/s, the rate of cartilage strain (i.e., net fluid exudation) was always significantly slower than the equivalent static loading strain rate (p < 0.0001, paired t-test). These values correspond to characteristic compression times τ on the order of 10 min during static compression versus 40 min at the start of 10 mm/s sliding, indicating that even slow sliding can 'buffer' (e.g., slow down) load-induced fluid exudation to a degree, although at such slow speeds the magnitude of recovery is not competitive with overall effect of compressive exudation.

With respect to interfacial friction, we confirmed that high-speed sliding in the cSCA consistently elicits exceptionally low equilibrium friction coefficients in PBS-lubricated contacts across all species and joints ($\mu_k \le 0.09$ at 80 mm/s, Figs. 6B & 7B), which mirrors all previous cSCA studies within bovine stifle cartilage [7,8,13–15]. Similarly, the presence of elevated peak frictions at the start of each intermittent sliding bout (Figs. 6A & 7A) parallels prior work [14,15,17]. All cSCA specimens exhibited high start-of-sliding friction coefficients (~0.1) regardless of sliding speed; however, when sliding speeds exceeded 30 mm/s, end-of-sliding μ_k values (analogous to equilibrium μ_k values) fell to between ~ 0.07 and ~ 0.005 (Fig. 6B). At intermediate speeds of 40-60 mm/s, robust, sliding-driven tribological rehydration facilitated characteristic friction recovery times $\tau < 1.5$ min (Fig. 8C). When slid at 80 mm/s, average characteristic friction recovery times dropped to \sim 30 s, highlighting the transient nature of the high friction environment seen at the start-of-sliding.

As an interface property, μ_k is typically understood to depend on the characteristics of and interactions between the glass counterface, lubricating solution (PBS), and cartilage surface [56]. The consistency of speed-dependent changes in friction among species and joints serves to highlight the apparent universal adaptation of cartilage's sliding surface to articulation. The contrasting matrix content and organizational characteristics among cartilage's distinct zones suggest diverging structure-function adaptations between the superficial zone, which constitutes the region of direct surface interaction, and the underlying deep zone [39]. Indeed, early experiments by McCutchen characterizing hydration-based lubrication found cartilage's lubrication response to be related to near-surface water content [1]. Such observations, in combination with the stratified, zonal composition of cartilage suggests clear structure-function relationships for optimizing its lubricating ability during articulation.

Recent comparative analyses of cartilage's microstructural features shed light on this phenomenon [19,20]. The relative thickness of cartilage's deep zone scales isometrically with body weight, while the middle and superficial zones scale with negative allometry, suggesting that the deep zone is primarily adapted to support increasing bodyweight [20]. And while compressive stiffness increases as a function of cartilage depth/zone [57,58], relative collagen and proteoglycan compositions within individual zones generally show no species (or body weight) dependency [19,20]. Similarly, numerous studies have shown superficial cartilage to be more dissipative and compliant than the bulk [58,59], and as a consequence, the predominate dissipator of shear energy [60].

From these observations, one can conclude, as Mancini et al. have, that evolutionary pressures have led to an optimized zonal composition and structure for shock absorption and load transfer within the stifle joint [20], with isometric scaling of deep zone cartilage thickness serving to support and transfer greater forces associated with increasing body weight. Extending Mancini's observations of microstructural similarity of superficial zone cartilage across species [20], one can reasonably suspect that unique evolutionary adaptations also exist for the superficial zone. Our findings of consistent articular cartilage rehydration and frictional behaviors among species combined with the established negative allometric scaling of the superficial zone suggest that the superficial zone's foremost function is to serve as a hydration-dependent bearing surface; subsequently, the superficial zone's load supporting capability appears to be an indirect consequence of the mechanism evolved to support such lubrication (activity-mediated near-surface

rehydration and interstitial lubrication recovery/sustenance). Furthermore, all available evidence points to a distinct, species-independent conservation of superficial zone structural and compositional characteristics that appears to optimize articular cartilage's tribomechanical function.

Despite consistent overall speed-dependent friction responses, we did observe quantifiable differences in friction outcomes among species. Both start- and end-of-sliding friction coefficients were lower for porcine specimens than the other species at all sliding speeds. In contrast, caprine specimens exhibited the highest start- and end-of-sliding friction coefficients, which exceeded porcine friction values by an order of magnitude. While the basis of this variance is not clear, these outcomes may be consequences of differences in intrinsic tissue quality/material properties or handling prior to their acquisition for testing. While all specimens were handled similarly upon arrival in the laboratory and determined to be both visually (free of macroscopic lesions or fissures) and tribologically acceptable, the tissues were acquired through different vendors/partners with potential consequences for tissue quality. For example, porcine and ovine joints were acquired directly from our abattoir partner, having been frozen within 48 h of slaughter; equine stifles from our veterinary partner were handled similarly. Bovine joints were acquired frozen following butchering, while our intact caprine stifle was procured from a local grocer, and thus its specific handling procedures were less clear. Cartilage friction is thought to depend on the composition of the articular surface, most notably the presence of lubricin, HA, and phospholipid-based surface coatings, which may vary based upon the handling [61-64]. Therefore, it is not surprising that friction magnitudes should vary among samples. Nonetheless, despite the undeniable presence of interspecies/inter-specimen variability in animal ages/sexes, contact geometries, cartilage thickness, material properties, etc., it is remarkable that all species and samples exhibited qualitatively consistent tribomechanical behaviors, both with regards to sliding-speed dependencies and outcome magnitudes. The fact that tribological rehydration did not vary markedly among species and samples suggests that the phenomenon is relatively insensitive to surface composition. Future studies will leverage the inherent variability observed among the present specimens to explore predictive relationships/correlations between intrinsic tissue properties (e.g., compressive modulus, permeability, etc.) and compression- and sliding-dependent tribomechanical performance.

Additionally, we note that through the opportunistic procurement of osteochondral specimens from several additional species/joints, we confirmed the existence of qualitatively consistent sliding-induced tribological rehydration behaviors across a broader range of mammalian and non-mammalian articular cartilage. These included forelimb cartilage samples from the bovine and porcine distal humerus, and ovine distal and proximal humerus; and hindlimb cartilage from ovine femoral head, domestic rabbit (O.c. domesticus) femoral condyles, white-tail deer (O. virginianuse) tarsals, and domestic chicken (G. gallus) and turkey (M. gallopavo) femoral condyles (data not shown). While these tests were of a 'one-off' variety, and in the case of the rabbit and chicken samples, approached the sensitivity limits of our reciprocal tribometer, these tests conclusively demonstrated sliding-induced tribological rehydration and sliding-mediated recovery of tribomechanical function to be universal in nature.

Finally, when we investigated the response of articular cartilage from different joints of a single porcine hindlimb, we found start- and end-of-sliding friction coefficients to be greater for porcine talar cartilage than stifle or femoral head cartilage at all speeds, a finding consistent with previous joint-specific characterization of cartilage [26]. Similarly, joint-specific variation in cartilage material properties is commonly observed, with talar cartilage being stiffer in compression and shear than femoral or tibial cartilage [23–26]. Contrasting mechanical properties among joints may reflect their biomechanical function: in the knee, articulation comprises sliding, rotation, rolling, and compression during gait, while articulation in the ankle primarily constitutes rolling

under high load [23]. Accordingly, it has been suggested, and our data support the interpretation, that talar cartilage's more robust compressive and superficial shear mechanics may be a preferential adaption for load transfer (as opposed to lubrication, although its frictional behaviors remain quite robust) [23,26]. Future studies are necessary to identify if such differences in the high-speed frictional responses are common among cSCA cartilage from different joints across other species.

5. Conclusion

This study demonstrated the exceptional consistency of tribological rehydration across mammalian articular cartilage. We showed, for the first time, the highly conserved nature of sliding speed-dependent compression and strain recovery in the cSCA (i.e., tribological rehydration) across species, although absolute compression recovery appears dictated by tissue thickness (i.e., varies with species). Our findings also highlight the ability of the cSCA to drive low, and often truly remarkable end-of-sliding friction values ($\mu_k << 0.1$) during PBS-lubricated, highspeed sliding tests in all species. Importantly, the notable similarity between speed-dependent end-of-sliding and time-averaged friction profiles across all species and specimens tested underscores the transient nature of high start-up frictions in the cSCA configuration, as opposed to the unmitigated (and non-physiological) increases in friction often seen in traditional SCA contacts. Together, these findings show the ability of articular cartilage to modulate its tissue compression, strain, and lubrication in response to sliding conditions consistent with normal joint articulation. This ability is both conserved among mammalian quadruped cartilage specimens and different joints, and likely represents a universal adaptation of articular cartilage tissue.

Declaration of Competing Interest

None.

Acknowledgements

This material was supported by the National Science Foundation (NSF) Biomechanics and Mechanobiology program [1635536]. Any opinions, findings, and conclusions expressed in this material are those of the authors and do not necessarily reflect the views of the NSF.

Appendix A. Supplementary data

Supplementary data to this article can be found online at https://doi.org/10.1016/j.biotri.2020.100159.

References

- [1] C.W. McCutchen, The frictional properties of animal joints, Wear 5 (1) (1962)1–17, https://doi.org/10.1016/0043-1648(62)90176-X.
- [2] M. Caligaris, G.A. Ateshian, Effects of sustained interstitial fluid pressurization under migrating contact area, and boundary lubrication by synovial fluid, on cartilage friction, Osteoarthr. Cartil. 16 (10) (2008) 1220–1227, https://doi.org/ 10.1016/j.joca.2008.02.020.
- [3] G.A. Ateshian, The role of interstitial fluid pressurization in articular cartilage lubrication, J. Biomech. 42 (9) (2009) 1163–1176, https://doi.org/10.1016/j. jbiomech.2009.04.040.
- [4] D.L. Burris, L. Ramsey, B.T. Graham, C. Price, A. Moore, How sliding and hydrodynamics contribute to articular cartilage fluid and lubrication recovery, Tribol. Lett. 67 (2019) 46, https://doi.org/10.1007/s11249-019-1158-7.
- [5] C.G. Armstrong, W.M. Lai, V.C. Mow, An analysis of the unconfined compression of articular cartilage, J. Biomech. Eng. 106 (2) (1984) 165–173, https://doi.org/ 10.1115/1.3138475.
- [6] V.C. Mow, C.C. Wang, C.T. Hung, The extracellular matrix, interstitial fluid and ions as a mechanical signal transducer in articular cartilage, Osteoarthr. Cartil. 7 (1) (1999) 41–58, https://doi.org/10.1053/joca.1998.0161.
- [7] A.C. Moore, D.L. Burris, Tribological rehydration of cartilage and its potential role in preserving joint health, Osteoarthr. Cartil. 25 (1) (2017) 99–107, https://doi. org/10.1016/j.joca.2016.09.018.
- [8] M.S. Farnham, R.E. Larson, D.L. Burris, C. Price, Effects of mechanical injury on the tribological rehydration and lubrication of articular cartilage, J Mech Behav

- Biomed Mater. 101 (103422) (2020), https://doi.org/10.1016/j.
- [9] F. Eckstein, M. Hudelmaier, R. Putz, The effects of exercise on human articular cartilage, J. Anat. 208 (4) (2006) 491–512, https://doi.org/10.1111/j.1469-7580 2006 00546 x
- [10] D.D. Chan, L. Cai, K.D. Butz, S.B. Trippel, E.A. Nauman, C.P. Neu, In vivo articular cartilage deformation: noninvasive quantification of intratissue strain during joint contact in the human knee, Sci. Rep. 6 (1) (2016) 19220, https://doi.org/10.1038/ sren19220.
- [11] J.L. Coleman, M.R. Widmyer, H.A. Leddy, et al., Diurnal variations in articular cartilage thickness and strain in the human knee, J. Biomech. 46 (2013) 541–547, https://doi.org/10.1016/j.jbiomech.2012.09.013.
- [12] R. Ekholm, B.E. Ingelmark, Functional thickness variations of human articular cartilage, Acta Soc. Med. Ups 57 (1–2) (1951) 39–59.
- [13] B.T. Graham, A.C. Moore, D.L. Burris, C. Price, Sliding enhances fluid and solute transport into buried articular cartilage contacts, Osteoarthr. Cartil. 25 (12) (2017) 2100–2107, https://doi.org/10.1016/j.joca.2017.08.014.
- [14] B.T. Graham, A.C. Moore, D.L. Burris, C. Price, Mapping the spatiotemporal evolution of solute transport in articular cartilage explants reveals how cartilage recovers fluid within the contact area during sliding, J. Biomech. 71 (11) (2018) 271–276, https://doi.org/10.1016/j.jbiomech.2018.01.041.
- [15] D.L. Burris, A.C. Moore, Cartilage and joint lubrication: new insights into the role of hydrodynamics, Biotribology 12 (2017) 8–14, https://doi.org/10.1016/J. BIOTRI.2017.09.001.
- [16] P.S. Walker, D. Dowson, M.D. Longfield, Wright4 V. "Boosted Lubrication" in Synovial Joints by Fluid Entrapment and Enrichment, Ann. Rheum. Dis. 27 (1968) 512. https://doi.org/10.1136/ard.27.6.512.
- [17] B.T. Graham, A.C. Moore, D.L. Burris, C. Price, Detrimental effects of long sedentary bouts on the biomechanical response of cartilage to sliding, Connect. Tissue Res. 61 (3-4) (2020) 375–388, https://doi.org/10.1080/ 03008207.2019.1673382.
- [18] E.D. Bonnevie, V.J. Baro, L. Wang, D.L. Burris, In situ studies of cartilage microtribology: roles of speed and contact area, Tribol. Lett. 41 (1) (2011) 83–95, https://doi.org/10.1007/s11249-010-9687-0.
- [19] J. Malda, J.C. de Grauw, K.E.M. Benders, et al., Of mice, men and elephants: the relation between articular cartilage thickness and body mass, PLoS One 8 (2) (2013), e57683, https://doi.org/10.1371/journal.pone.0057683.
- [20] I.A.D. Mancini, L. Rieppo, B. Pouran, et al., Effects of body mass on microstructural features of the osteochondral unit: a comparative analysis of 37 mammalian species, Bone (July 2019), https://doi.org/10.1016/J.BONE.2019.07.001.
- [21] K.A. Athanasiou, M.P. Rosenwasser, J.A. Buckwalter, T.I. Malinin, V.C. Mow, Interspecies comparisons of in situ intrinsic mechanical properties of distal femoral cartilage, J. Orthop. Res. 9 (3) (1991) 330–340, https://doi.org/10.1002/ jor.1100090304.
- [22] N.L. Fetter, H.A. Leddy, F. Guilak, J.A. Nunley, Composition and transport properties of human ankle and knee cartilage, J. Orthop. Res. 24 (2) (2006) 211–219, https://doi.org/10.1002/jor.20029.
- [23] S. Treppo, S. Koepp, E.C. Quan, A.A. Cole, K.E. Kuettner, A.J. Grodzinsky, Comparison of biomechanical and biochemical properties of cartilage from human knee and ankle pairs, J. Orthop. Res. 8 (2000) 739–748, https://doi.org/10.1002/ jor_1100180510
- [24] T.M. Quinn, H. Häuselmann, N. Shintani, E.B. Hunziker, Cell and matrix morphology in articular cartilage from adult human knee and ankle joints suggests depth-associated adaptations to biomechanical and anatomical roles, Osteoarthr. Cartil. 21 (12) (2013) 1904–1912, https://doi.org/10.1016/j.joca.2013.09.011.
- [25] J.P.A. Arokoski, M.M. Hyttinen, H.J. Helminen, J.S. Jurvelin, Biomechanical and structural characteristics of canine femoral and tibial cartilage, J. Biomed. Mater. Res. 48 (2) (1998) 99–107, https://doi.org/10.1002/(SICI)1097-4636(1999)48: 2<99::AID-JBM1>3.0.CO;2-N.
- [26] C.R. Henak, K.A. Ross, E.D. Bonnevie, et al., Human talar and femoral cartilage have distinct mechanical properties near the articular surface, J. Biomech. 49 (14) (2016) 3320–3327, https://doi.org/10.1016/J.JBIOMECH.2016.08.016.
- [27] A.C. Moore, D.L. Burris, Tribological and material properties for cartilage of and throughout the bovine stifle: support for the altered joint kinematics hypothesis of osteoarthritis, Osteoarthr. Cartil. 23 (1) (2015) 161–169, https://doi.org/10.1016/ j.joca.2014.09.021.
- [28] A.C. Moore, J.L. Schrader, J.J. Ulvila, D.L. Burris, A review of methods to study hydration effects on cartilage friction, Tribol. Mater. Surf. Interf. 11 (4) (2017) 202–214, https://doi.org/10.1080/17515831.2017.1397329.
- [29] R.L.-Y. Sah, Y.-J. Kim, J.-Y.H. Doong, A.J. Grodzinsky, K Plaas AH, Sandy JD., Biosynthetic response of cartilage explants to dynamic compression, J. Orthop. Res. 7 (1989) 619–636, https://doi.org/10.1002/jor.1100070502.
- [30] D. Bates, M. Mächler, B.M. Bolker, S.C. Walker, Fitting linear mixed-effects models using lme4, J. Stat. Softw. 67 (1) (2015), https://doi.org/10.18637/jss.v067.i01.
- [31] Linear Mixed-Effects Models: Basic Concepts and Examples, in: Mixed-Effects Models in Sand S-PLUS, Springer New York, New York, NY, 2000, pp. 3–56, https://doi.org/10.1007/978-1-4419-0318-1_1.
- [32] X.A. Harrison, L. Donaldson, M.E. Correa-Cano, et al., A brief introduction to mixed effects modelling and multi-model inference in ecology, PeerJ. 2018 (5) (2018) 1–32. https://doi.org/10.7717/peeri.4794.
- [33] F. Eckstein, M. Tieschky, S. Faber, K.H. Englmeier, M. Reiser, Functional analysis of articular cartilage deformation, recovery, and fluid flow following dynamic exercise in vivo, Anat. Embryol. (Berl). 200 (4) (1999) 419–424. http://www.ncbi. nlm.nih.gov/pubmed/10460479 (Accessed July 23, 2019).

- [34] N.K. Lad, B. Liu, P.K. Ganapathy, et al., Effect of normal gait on in vivo tibiofemoral cartilage strains, J. Biomech. 49 (13) (2016) 2870–2876, https://doi. org/10.1016/J.JBIOMECH.2016.06.025.
- [35] S. Gilbert, T. Chen, I.D. Hutchinson, et al., Dynamic contact mechanics on the tibial plateau of the human knee during activities of daily living, J. Biomech. 47 (9) (2014) 2006–2012, https://doi.org/10.1016/j.jbiomech.2013.11.003.
- [36] P. Vakiel, M. Shekarforoush, C.R. Dennison, et al., Stress measurements on the articular cartilage surface using fiber optic technology and in-vivo gait kinematics, Ann. Biomed. Eng. (2020), https://doi.org/10.1007/s10439-020-02516-x.
- [37] P. Vakiel, M. Shekarforoush, C.R. Dennison, et al., Mapping stresses on the Tibial plateau cartilage in an ovine model using in-vivo gait kinematics, Ann. Biomed. Eng. (2020), https://doi.org/10.1007/s10439-020-02650-6.
- [38] G.A. Ateshian, H.Q. Wang, W.M. Lai, The role of interstitial fluid pressurization and surface porosities on the boundary friction of articular cartilage, J. Tribol. 120 (2) (1998) 241–248, https://doi.org/10.1115/1.2834416.
- [39] G.A. Ateshian, C.T. Hung, The natural synovial joint: properties of cartilage, Proc. Inst. Mech. Eng. Part J J. Eng. Tribol. 220 (8) (2006) 657–670, https://doi.org/ 10.1243/13506501JET86.
- [40] R.A. Brand, Joint contact stress: a reasonable surrogate for biological processes? Iowa Orthop. J. 25 (2005) 82–94.
- [41] J.P. Gleghorn, L.J. Bonassar, Lubrication mode analysis of articular cartilage using Stribeck surfaces, J. Biomech. 41 (9) (2008) 1910–1918, https://doi.org/10.1016/ j.jbiomech.2008.03.043.
- [42] R. Krishnan, M. Caligaris, R.L. Mauck, C.T. Hung, K.D. Costa, G.A. Ateshian, Removal of the superficial zone of bovine articular cartilage does not increase its frictional coefficient, Osteoarthr. Cartil. 12 (12) (2004) 947–955, https://doi.org/ 10.1016/j.joca.2004.08.009.
- [43] I.M. Basalo, R.L. Mauck, T.A.N. Kelly, et al., Cartilage interstitial fluid load support in unconfined compression following enzymatic digestion, J. Biomech. Eng. 126 (6) (2004) 779–786, https://doi.org/10.1115/1.1824123.
- [44] E.D. Bonnevie, M.L. Delco, D. Galesso, C. Secchieri, L.A. Fortier, L.J. Bonassar, Subcritical impact inhibits the lubricating mechanisms of articular cartilage, J. Biomech. 53 (2017) 64–70, https://doi.org/10.1016/j.jbiomech.2016.12.034.
- [45] J.P. Gleghorn, A.R.C. Jones, C.R. Flannery, L.J. Bonassar, Alteration of articular cartilage frictional properties by transforming growth factor β, interleukin-1β, and oncostatin M, Arthritis Rheum. 60 (2) (2009) 440–449, https://doi.org/10.1002/ art.24259.
- [46] C.J. Bell, E. Ingham, J. Fisher, Influence of hyaluronic acid on the time-dependent friction response of articular cartilage under different conditions, Proc. Inst. Mech. Eng. Part H J. Eng. Med. 220 (1) (2006) 23–31, https://doi.org/10.1243/ 095441105X69060.
- [47] M.J. Hossain, H. Noori-Dokht, S. Karnik, et al., Anisotropic properties of articular cartilage in an accelerated in vitro wear test, J. Mech. Behav. Biomed. Mater. 109 (2020), https://doi.org/10.1016/j.jmbbm.2020.103834.
- [48] V.C. Mow, The role of lubrication in biomechanical joints, J. Biomech. Eng. (1969) 320–326, https://doi.org/10.1115/1.3554924.
- [49] M. Shekarforoush, J.E. Beveridge, D.A. Hart, C.B. Frank, N.G. Shrive, Correlation between translational and rotational kinematic abnormalities and osteoarthritislike damage in two in vivo sheep injury models, J. Biomech. 75 (2018) 67–76, https://doi.org/10.1016/j.jbiomech.2018.04.046.

- [50] M. Shekarforoush, P. Vakiel, M. Scott, G. Muench, D.A. Hart, N.G. Shrive, Relative surface velocity of the tibiofemoral joint and its relation to the development of osteoarthritis after joint injury, Ann. Biomed. Eng. 48 (2) (2020) 695–708, https:// doi.org/10.1007/s10439-019-02392-0.
- [51] L. St. George, S.H. Roy, J. Richards, J. Sinclair, S.J. Hobbs, Surface EMG signal normalisation and filtering improves sensitivity of equine gait analysis, Comp. Exerc. Physiol. 15 (3) (2019) 173–185, https://doi.org/10.3920/CEP190028.
- [52] K.Z. Takahashi, T.M. Kepple, S.J. Stanhope, A unified deformable (UD) segment model for quantifying total power of anatomical and prosthetic below-knee structures during stance in gait, J. Biomech. 45 (15) (2012) 2662–2667, https:// doi.org/10.1016/j.jbiomech.2012.08.017.
- [53] L.G. Faria, S.C. Rahal, F.S. Agostinho, et al., Kinematic analysis of forelimb and hind limb joints in clinically healthy sheep, BMC Vet. Res. 10 (294) (2014), https://doi.org/10.1186/s12917-014-0294-4.
- [54] M. Shekarforoush, K.I. Barton, J.E. Beveridge, et al., Alterations in joint angular velocity following traumatic knee injury in ovine models, Ann. Biomed. Eng. 47 (3) (2019) 790–801, https://doi.org/10.1007/s10439-019-02203-6.
- [55] S. Patil, N. Steklov, L. Song, W.C. Bae, D.D. D'Lima, Comparative biomechanical analysis of human and caprine knee articular cartilage, Knee 21 (1) (2014) 119–125, https://doi.org/10.1016/j.knee.2013.03.009.
- [56] A.C. Dunn, W.G. Sawyer, T.E. Angelini, Gemini interfaces in aqueous lubrication with hydrogels, Tribol. Lett. 54 (1) (2014) 59–66, https://doi.org/10.1007/ s11249-014-0308-1.
- [57] R.C. Stewart, A.N. Patwa, H. Lusic, et al., Synthesis and preclinical characterization of a cationic iodinated imaging contrast agent (CA4+) and its use for quantitative computed tomography of ex vivo human hip cartilage, J. Med. Chem. 60 (2017) 5543–5555, https://doi.org/10.1021/acs.jmedchem.7b00234.
- [58] M.R. Buckley, A.J. Bergou, J. Fouchard, L.J. Bonassar, I. Cohen, High-resolution spatial mapping of shear properties in cartilage, J. Biomech. 43 (4) (2010) 796–800, https://doi.org/10.1016/j.jbiomech.2009.10.012.
- [59] R.M. Schinagl, D. Gurskis, A.C. Chen, R.L. Sah, Depth-dependent confined compression modulus of full-thickness bovine articular cartilage, J. Orthop. Res. 15 (4) (1997) 499–506, https://doi.org/10.1002/jor.1100150404.
- [60] M.R. Buckley, C. CH, L.J. Bonassar, Localization of viscous behavior and shear energy dissipation in articular cartilage under dynamic shear loading, J. Biomech. Eng. 135 (031002) (2013), https://doi.org/10.1115/1.4007454.
- [61] E.D. Bonnevie, D. Galesso, C. Secchieri, I. Cohen, L.J. Bonassar, Elastoviscous transitions of articular cartilage reveal a mechanism of synergy between lubricin and hyaluronic acid, PLoS One 10 (11) (2015) 1–15, https://doi.org/10.1371/ journal.pone.0143415.
- [62] P.S. Walker, A. Unsworth, D. Dowson, J. Sikorski, V. Wright, Mode of aggregation of hyaluronic acid protein complex on the surface of articular cartilage, Ann. Rheum. Dis. 29 (6) (1970) 591–602, https://doi.org/10.1136/ard.29.6.591.
- [63] H.L. Reesink, E.D. Bonnevie, S. Liu, et al., Galectin-3 binds to Lubricin and reinforces the lubricating boundary layer of articular cartilage, Sci. Rep. 6 (1) (2016) 25463. https://doi.org/10.1038/srep.25463.
- [64] S. Sivan, A. Schroeder, G. Verberne, et al., Liposomes act as effective biolubricants for friction reduction in human synovial joints, Langmuir 26 (2) (2010) 1107–1116, https://doi.org/10.1021/la9024712.